COMMUNICATIONS IN COMPUTATIONAL PHYSICS
Vol. **4**, No. 5, pp. 1034-1050

Commun. Comput. Phys.
November 2008

Stationary and Transient Simulations for a One-Dimensional Resonant Tunneling Diode†

Xin Hu[1,2], Shaoqiang Tang[1,*] and Maxime Leroux[3]

[1] *CAPT, College of Engineering, Peking University, Beijing 100871, China.*
[2] *Applied and Computational Mathematics, California Institute of Technology, Pasadena, CA 91125, USA.*
[3] *Department of Physics, ENS de Lyon, 69364 Lyon cedex 07, France.*

Received 7 March 2008; Accepted (in revised version) 25 May 2008

Available online 10 July 2008

Abstract. We investigate the validity of stationary simulations for semiconductor quantum charge transport in a one-dimensional resonant tunneling diode via fluid type models. Careful numerical investigations to a quantum hydrodynamic model reveal that the transient simulations do not always converge to the steady states. In particular, growing oscillations are observed at relatively large applied voltage. A dynamical bifurcation is responsible for the stability interchange of the steady state. Transient and stationary computations are also performed for a unipolar quantum drift-diffusion model.

PACS: 02.60.Cb, 73.63.-b, 02.30.Jr

Key words: Quantum effects, charge transport, dissipation, transient/stationary computation.

1 Introduction

Miniaturization of semiconductor devices maintains a continuing trend in microelectronics industry, approaching the nanometer length scale [15]. In the modeling and simulations for nano-devices, it is crucial to incorporate the quantum effects in a proper manner. Because a complete description at the quantum mechanics level would require immense computing power, one usually makes a compromise between the numerical cost and the modeling accuracy. Due to their simplicity in formulation and similarity to the governing equations for classical devices, fluid type models have been widely explored, both theoretically and numerically [16, 20, 21]. However, these models involve strong nonlinearity

†Dedicated to Professor Xiantu He on the occasion of his 70th birthday.
*Corresponding author. *Email addresses:* lanxin@acm.caltech.edu (X. Hu), maotang@pku.edu.cn (S. Tang), maxime.leroux@ens-lyon.fr (M. Leroux)

and high order spatial derivatives representing quantum effects. Rigorous mathematical analysis are desirable and challenging. We refer to [1, 17, 19, 22] and references therein for more details. There then arises an urgent demand to justify fluid type models, which are typically derived in a formal way using closure assumptions, temporal and spatial scalings, etc. Careful numerical studies are an indispensable tool to serve this purpose, namely, to validate a model or to identify its effective range.

In this paper, we are concerned with the dynamical stability of steady states for fluid type models. To be more specific, we take a resonant tunneling diode (RTD) in one space dimension to investigate a quantum hydrodynamic (QHD) model, and a quantum drift-diffusion (QDD) model. RTD is a simple device that bears distinct quantum features. With a double potential barrier, the electric current decreases when the applied voltage increases in a certain range. This negative differential resistance (NDR) is caused by the quantum tunneling effect. Comparing transient and stationary QHD simulations, we observe that the steady states lose dynamical stability at moderate applied voltage. At a higher voltage, the transient solutions exhibit both spatial and temporal oscillations. Even the average current density differs from the stationary computations. A dynamical bifurcation occurs for the governing partial differential equations. The role of dissipation is a common issue for discussing instabilities. Actually, interplay between the quantum mechanism and the dissipative mechanism has been explored in a viscous quantum hydrodynamic (vQHD) model [17, 18]. On the other hand, steady states are stable in all our numerical experiments for the QDD model, where the diffusion dominates. However, the QDD model fails to reproduce the NDR phenomenon.

This study poses, likely for the first time, a question on whether stationary computations are always reliable in producing the current-voltage (I-V) curves for nano devices. As a matter of fact, almost all semiconductor quantum charge transport simulations have been performed with stationary problems, e.g. by using the Gummel iterations [8, 13, 23].

The rest of the paper is organized as follows. First, we sketch the derivation for the QHD model and the QDD model in Section 2. Then we describe the numerical algorithm for the QHD model in Section 3, and some numerical results are presented in Section 4. We briefly discuss the numerical scheme and simulations for the QDD model in Section 5. Finally, we make some further discussions in Section 6.

2 QHD model

Dynamics of carrier transport is governed by the Wigner-Poisson system at the quantum level [10, 21]:

$$\frac{\partial w}{\partial t}+\frac{p}{m}\cdot\nabla_x w+\frac{q}{m}\theta[V](w)=Q(w), \tag{2.1}$$

$$\varepsilon_s\triangle V=q\left(\int_{\mathbb{R}} w\mathrm{d}p-C(x)\right), \tag{2.2}$$

where the pseudo-differential operator is defined by

$$\begin{aligned}&\theta[V](w)(x,p,t)\\&=\frac{i}{(2\pi)^d}\int_{\mathbb{R}^{2d}}\frac{m}{\hbar^2}\left[V(x+\frac{\eta}{2},t)-V(x-\frac{\eta}{2},t)\right]\times w(x,p',t)e^{i(p-p')\eta/\hbar}dp'd\eta.\end{aligned}$$

Here $w(x,p,t)$ and $V(x,t)$ are the Wigner function and electrostatic potential, respectively. The independent variables are $x\in\mathbb{R}^d$ for the space, $p\in\mathbb{R}^d$ for the momentum, and t for the time. The physical constants and parameters include the reduced Planck constant $\hbar=1.0546\times10^{-34}\text{kgm}^2/\text{s}$, Boltzmann constant $k_B=1.3807\times10^{-23}\text{kgm}^2/\text{s}^2\text{K}$, effective electron mass $m=0.0607\times10^{-31}\text{kg}$, elementary charge $q=1.602\times10^{-19}\text{As}$ and semiconductor permittivity $\varepsilon_s=12.9\times8.8542\times10^{-12}\ \text{A}^2\text{s}^4/\text{kgm}^3$. The doping concentration $C(x)$ is material and device dependent, and shall be specified later for RTD. The collision operator $Q(w)$ represents the interaction among different quantum states. We assume that it conserves the first three momenta, i.e.

$$\int_{\mathbb{R}^d}Q(w)\kappa(p)\mathrm{d}p=0,\quad\text{for}\quad\kappa(p)=(1,p/m,|p|^2/2m). \tag{2.3}$$

We define the macroscopic particle density $n(x,t)$, current density $J(x,t)$ and energy density $e(x,t)$ by

$$(n,J,e)=\int_{\mathbb{R}^d}f(x,p,t)\kappa(p)\mathrm{d}p. \tag{2.4}$$

Multiplying $\kappa(p)$ to (2.1) and integrating over $p\in\mathbb{R}^d$, we obtain a system

$$\partial_t n+\nabla\cdot J=0, \tag{2.5}$$

$$\partial_t J+\nabla\cdot\left(\frac{J\otimes J}{n}+P\right)-n\nabla V=0, \tag{2.6}$$

$$\partial_t e+\nabla\cdot\left((P+eI)\cdot\frac{J}{n}+S\right)-J\cdot\nabla V=0. \tag{2.7}$$

In order to find the constitutive relations for the stress tensor P and quantum thermal flux S, we follow [9, 17] and assume that the temperature varies slowly in space, and the device has spatial and temporal scales much larger than the quantum characteristic scales. Then we find that

$$P=\frac{k_B}{m}nTI-\frac{\hbar^2}{12m^2}n(\nabla\otimes\nabla)\log n, \tag{2.8}$$

and

$$S=\frac{\hbar^2}{8m^2}n\triangle\left(\frac{J}{n}\right). \tag{2.9}$$

Following [11], we include a thermal diffusion term $k_B\sigma/m\nabla\cdot(n\nabla T)$. Here the coefficient $\sigma=0.2\tau_0k_BT_0/m$, with a relaxation time $\tau_0=0.9\times10^{-12}\text{s}$ and a lattice temperature $T_0=77\text{K}$.

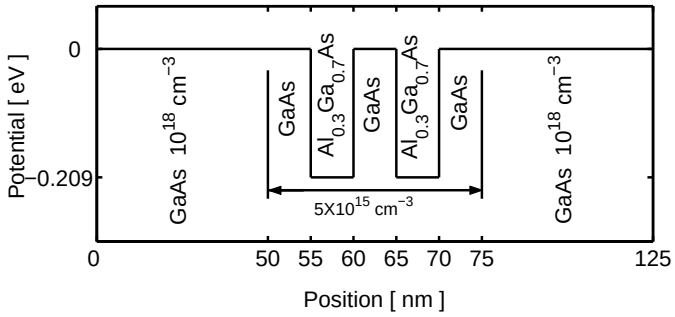

Figure 1: Geometry of RTD and potential barrier.

We further make a potential modification. In a one dimensional RTD as shown in Fig. 1, there is a quasi-Fermi energy shift due to the double potential barrier

$$B(x)=\begin{cases} -0.209\,\text{eV}, & \text{for } x\in[55\text{nm},60\text{nm}]\cup[65\text{nm},70\text{nm}],\\ 0\,\text{eV}, & \text{elsewhere.}\end{cases} \tag{2.10}$$

Meanwhile, the doping profile for this RTD is

$$C(x)=\begin{cases} 5\times10^{15}\text{cm}^3, & \text{for } x\in[50\text{nm},75\text{nm}],\\ 10^{18}\text{cm}^3, & \text{elsewhere.}\end{cases} \tag{2.11}$$

In summary, the QHD model for a one-dimensional RTD reads as follows:

$$n_t+J_x=0, \tag{2.12}$$

$$J_t+\left(\frac{J^2}{n}\right)_x+\frac{k_B}{m}(nT)_x-\frac{q}{m}n(V+B(x))_x-\frac{\hbar^2}{6m^2}n\left(\frac{(\sqrt{n})_{xx}}{\sqrt{n}}\right)_x=0, \tag{2.13}$$

$$\begin{aligned} e_t+&\left[\frac{5k_B}{2m}TJ+\frac{J^3}{2n^2}-\frac{\hbar^2}{8m^2}\left(J(\log n)_{xx}+n\left(\frac{J}{n}\right)_{xx}\right)\right]_x\\ &-\frac{q}{m}J(V+B(x))_x=\frac{k_B\sigma}{m}(nT_x)_x, \end{aligned} \tag{2.14}$$

$$\varepsilon_s V_{xx}=q(n-C(x)). \tag{2.15}$$

To make a comparison, we mention that a vQHD model may be derived in a similar manner from a viscous Wigner-Fokker-Planck equation [2,18]:

$$n_t+J_x=D_{qq}n_{xx}, \tag{2.16}$$

$$\begin{aligned} J_t+&\left(\frac{J^2}{n}\right)_x+\frac{k_B}{m}\left(1+\frac{D_{pq}}{k_BT_0}\right)(nT_0)_x-\frac{q}{m}n(V+B(x))_x\\ &-\frac{\hbar^2}{6m^2}n\left(\frac{(\sqrt{n})_{xx}}{\sqrt{n}}\right)_x=-\frac{J}{\tau_0}+D_{qq}J_{xx}, \end{aligned} \tag{2.17}$$

$$\varepsilon_s V_{xx}=q(n-C(x)). \tag{2.18}$$

Here the energy equation is not included, and additional quantum terms appeared with coefficients

$$D_{pq}=\frac{\hbar^2}{6\pi k_B T_0 \tau_0}, \quad D_{qq}=\frac{\hbar^2}{12 m k_B T_0 \tau_0}.$$

Furthermore, we may derive the standard quantum drift-diffusion (QDD) equations by considering the limit $\tau_0 \to 0$ in the inviscid system (with $D_{pq}=D_{qq}=0$):

$$n_t + J_x = 0, \tag{2.19}$$

$$\frac{k_B}{m}(nT_0)_x - \frac{q}{m}n(V+B(x))_x - \frac{\hbar^2}{6m^2}n\left(\frac{(\sqrt{n})_{xx}}{\sqrt{n}}\right)_x = -\frac{J}{\tau_0}, \tag{2.20}$$

$$\varepsilon_s V_{xx} = q(n - C(x)). \tag{2.21}$$

3 Numerical algorithms for QHD computations

We describe the numerical algorithms in three parts, namely, the transient simulation, the stationary simulation, and initial data preparation.

3.1 A central difference scheme for transient computations

An admissible weak solution for a standard fluid system is usually obtained through a vanishing viscosity approach. As is well-known, a hyperbolic solver introduces numerical viscosity around sharp gradients (or discontinuities). The numerical viscosity coefficient decreases when we refine the mesh. Accordingly, in numerical simulations with such a solver, a finer mesh usually yields better resolution at discontinuities. In contrast, complexity due to the interplay between the quantum mechanism and the dissipations was revealed in careful numerical explorations on RTD with the vQHD model [18]. In Fig. 2, we observe that even the current density, an averaged quantity, has a big difference at two small viscosity coefficients. Simulation results demonstrate that the numerical solution under decreasing viscosity does not converge, and further indicates that the (inviscid) QHD model (without energy equation) is likely not well-posed. Hence we would not expect reliable and robust simulations for the QHD model. This may shed insight to the difficulties occurred in earlier numerical simulations [3,5–7], where quite different I-V curves were reported for essentially the same RTD device. We notice that an I-V curve is the key output for device simulations, passed to circuit simulations for chip design and analysis.

To avoid artifacts corresponding to the numerical viscosity, we adopt a central difference scheme for the transient QHD computations.

We make a uniform discretization $x_i = i\triangle x$, $i=0,\cdots,N$, with $\triangle x = L/N$ the mesh size, and $L=125$nm the device length. The primary numerical variables are

$$n_i(t)=n(x_i,t), \quad e_i(t)=e(x_i,t), \quad V_i(t)=V(x_i,t), \quad J_{i-1/2}=J(x_{i-1/2},t).$$

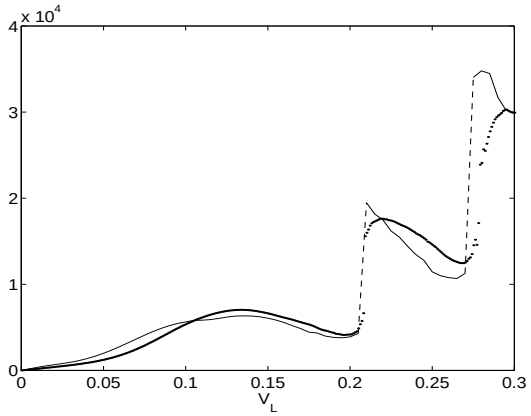

Figure 2: Effective current density (in A/cm^{-2}) versus applied voltage (in V) by vQHD simulations with two viscosity constants: normal D_{qq} (thin solid line) and double D_{qq} (thick dotted line).

We adopt the standard second order Runge-Kutta method to solve the following semi-discrete equations:

$$\frac{\mathrm{d}n_i}{\mathrm{d}t}=-\frac{J_{i+1/2}-J_{i-1/2}}{\triangle x},\quad i=1,\cdots,N-1, \tag{3.1}$$

$$\begin{aligned}\frac{\mathrm{d}J_{i-1/2}}{\mathrm{d}t}=&-\frac{1}{\triangle x}\left(\frac{J_i^2}{n_i}-\frac{J_{i-1}^2}{n_{i-1}}\right)-\frac{k_B}{m\triangle x}(n_iT_i-n_{i-1}T_{i-1})\\&+\frac{qn_{i-1/2}}{m\triangle x}\Big[(V_i+B(x_i))-(V_{i-1}+B(x_{i-1}))\Big]+\frac{\hbar^2n_{i-1/2}}{6m^2\triangle x}(P_i-P_{i-1}),\quad i=1,\cdots,N,\end{aligned} \tag{3.2}$$

$$\begin{aligned}\frac{\mathrm{d}e_i}{\mathrm{d}t}=&-\frac{5k_B}{2m\triangle x}(J_{i+1/2}T_{i+1/2}-J_{i-1/2}T_{i-1/2})-\frac{1}{2\triangle x}\left(\frac{J_{i+1/2}^3}{n_{i+1/2}}-\frac{J_{i-1/2}^3}{n_{i-1/2}}\right)\\&\times\frac{qJ_i}{m\triangle x}\Big[(V_{i+1/2}+B(x_{i+1/2}))-(V_{i-1/2}+B(x_{i-1/2}))\Big]+\frac{\hbar^2}{8m^2\triangle x}(Q_{i+1/2}-Q_{i-1/2})\\&+\frac{k_B\sigma}{(\triangle x)^2}\Big[n_{i+1/2}(T_{i+1}-T_i)-n_{i-1/2}(T_i-T_{i-1})\Big],\quad i=1,\cdots,N-1,\end{aligned} \tag{3.3}$$

$$0=\epsilon_s\frac{V_{i+1}-2V_i+V_{i-1}}{(\triangle x)^2}-q(n_i-C(x_i)),\quad i=1,\cdots,N-1. \tag{3.4}$$

Here, P_i and $Q_{i+1/2}$ are the discrete quantum terms

$$P_i=\frac{1}{\triangle x}\left(\sqrt{\frac{n_{i+1}}{n_i}}+\sqrt{\frac{n_{i-1}}{n_i}}-2\right), \tag{3.5}$$

$$\begin{aligned}Q_{i+1/2}=&\frac{J_{i+1/2}}{(\triangle x)^2}(\log n_{i+3/2}-2\log n_{i+1/2}+\log n_{i-1/2})\\&+\frac{n_{i+1/2}}{(\triangle x)^2}\left(\frac{J_{i+3/2}}{n_{i+3/2}}-2\frac{J_{i+1/2}}{n_{i+1/2}}+\frac{J_{i-1/2}}{n_{i-1/2}}\right).\end{aligned} \tag{3.6}$$

We use $J_i=(J_{i-1/2}+J_{i+1/2})/2$, $n_{i+1/2}=(n_i+n_{i+1})/2$ and similar for other variables.

Furthermore, Ohmic contact boundary conditions are imposed [3]:

$$n(0)=C(0),\quad n(L)=C(L),\quad n_x(0)=n_x(L)=0,$$
$$J_x(0)=J_x(L)=0,\quad T(0)=T(L)=T_0,\quad V(0)=0,\quad V(L)=\mathrm{V}_B.$$

3.2 A central difference scheme for stationary computations

Discarding the temporal derivatives in (2.12)-(2.15), we obtain the ODE system that describes the steady states. The first equation may be readily integrated once, which implies a constant current density

$$J(x)=J_0. \tag{3.7}$$

Then we solve by the Newton-Raphson method the following nonlinear algebraic system:

$$\begin{aligned}0=&-\frac{1}{\triangle x}\left(\frac{J_0^2}{n_i}-\frac{J_0^2}{n_{i-1}}\right)-\frac{k_B}{m\triangle x}(n_iT_i-n_{i-1}T_{i-1}) \\ &+\frac{qn_{i-1/2}}{m\triangle x}\Big[(V_i+B(x_i))-(V_{i-1}+B(x_{i-1}))\Big]+\frac{\hbar^2n_{i-1/2}}{6m^2\triangle x}(P_i-P_{i-1}),\quad i=0,\cdots,N-1,\end{aligned} \tag{3.8}$$

$$\begin{aligned}0=&-\frac{5k_B}{2m\triangle x}(J_0T_{i+1/2}-J_0T_{i-1/2})-\frac{1}{2\triangle x}\left(\frac{J_0^3}{n_{i+1/2}}-\frac{J_0^3}{n_{i-1/2}}\right) \\ &\times\frac{qJ_0}{m\triangle x}\Big[(V_{i+1/2}+B(x_{i+1/2}))-(V_{i-1/2}+B(x_{i-1/2}))\Big]+\frac{\hbar^2}{8m^2\triangle x}(Q_{i+1/2}-Q_{i-1/2}) \\ &+\frac{k_B\sigma}{(\triangle x)^2}\Big[n_{i+1/2}(T_{i+1}-T_i)-n_{i-1/2}(T_i-T_{i-1})\Big],\quad i=1,\cdots,N-1,\end{aligned} \tag{3.9}$$

$$0=\frac{V_{i+1}-2V_i+V_{i-1}}{(\triangle x)^2}-\frac{q}{\epsilon_s}(n_i-C(x_i)),\quad i=1,\cdots,N-1. \tag{3.10}$$

Here the quantum terms are

$$P_i=\frac{1}{\triangle x}\left(\sqrt{\frac{n_{i+1}}{n_i}}+\sqrt{\frac{n_{i-1}}{n_i}}-2\right), \tag{3.11}$$

$$\begin{aligned}Q_{i+1/2}=&\frac{J_0}{(\triangle x)^2}(\log n_{i+3/2}-2\log n_{i+1/2}+\log n_{i-1/2}) \\ &+\frac{n_{i+1/2}}{(\triangle x)^2}\left(\frac{J_0}{n_{i+3/2}}-2\frac{J_0}{n_{i+1/2}}+\frac{J_0}{n_{i-1/2}}\right).\end{aligned} \tag{3.12}$$

3.3 Initial data preparation and continuation strategy

The nonlinear interaction between the quantum mechanism and the convection/diffusion terms is a delicate issue. The quantum terms involve high order derivatives, and a strong

initial layer appears in the transient computations. If the initial data is not well prepared, the initial layer can be so strong that the numerical simulation breaks almost immediately. Similarly, to solve the nonlinear algebraic system, the stationary computations also require a well-prepared initial guess.

We compute the transient solution for zero applied voltage $V_B = 0$ in the following way. First, we ignore the potential barrier and take a classical hydrodynamic model, namely, with $B(x) = 0$ and $\hbar = 0$. Without the quantum terms, a transient computation may be readily performed, and the numerical solution converges toward the steady state. Next, we gradually increase $\hbar$ from 0 to the true physical value in 10 sub-steps. At each sub-step, we use the steady state to the previous choice of $\hbar$ as the initial data. Using the solution with the true physical value of $\hbar$, we compute corresponding steady states with gradually increasing barrier height in a similar way, until it reaches 0.209V. In this manner, we obtain the asymptotic solution to the transient QHD system at zero applied voltage.

We use this solution as the initial guess for the Newton-Raphson code at $V_B = 0$. In particular, we take the average current density (in space) as the initial guess for J_0. The stationary computations then adopt a continuation strategy. That is, we iterate until the stationary solution is obtained at a certain applied voltage V_B. We then use this steady state as the initial guess for the iterations at applied voltage $V_B + \triangle V_B$. In simulations presented hereafter, we take $\triangle V_B = 0.1$mV. By this procedure, we obtain the steady states for applied voltages in the range of $[0, 0.22\text{V}]$.

Finally, we perform transient computations at selected V_B's, using the steady states at each V_B as the initial data. We remark that a numerical stationary solution solves the nonlinear algebraic system, whereas a numerical transient solution solves the semi-discrete ODE system. There is a difference in the formulation, which generates initial layers in a transient computation. The deviation also provides a perturbation to a steady state, which is desirable for dynamical stability check.

4 Numerical results for the QHD model

Simulations with the QHD model are summarized in Fig. 3. We use 500 grid points to resolve the space. The transient computations are performed with a time step size $\triangle t = 10^{-5}$ps. We terminate the computations typically up to several hundred picosecond, or when a steady state is reached. We remark that the same stationary results were reported in [17] for a larger range of applied voltage, by a damped Newton method to solve the nonlinear algebraic system.

There are two distinct features in Fig. 3. First, the negative differential resistance (NDR) is captured. NDR occurs when V_B goes beyond a threshold at around 0.18V. The threshold and corresponding current densities are slightly different from the vQHD results in Fig. 2. The other feature, which we shall describe in more details is the obvious difference in the transient and stationary computations.

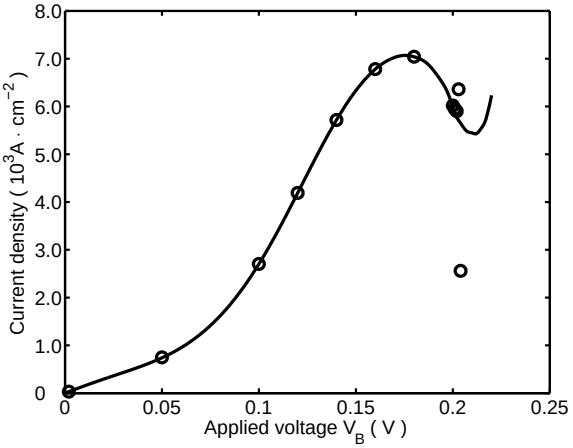

Figure 3: I-V curve: stationary computations (solid), and transient computations (circles).

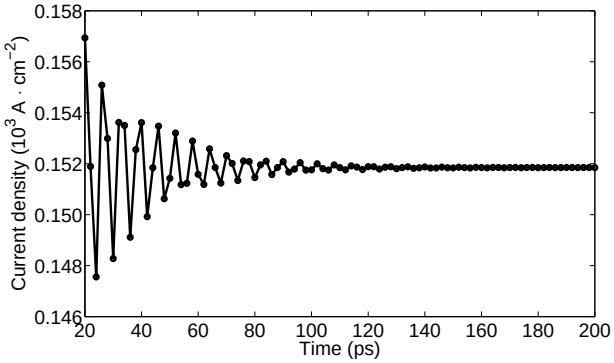

Figure 4: Current density (averaged in space) by transient computations at $V_B = 0.01$V.

When the applied voltage is small, the transient solution gradually converges to the corresponding steady state. This is illustrated in Fig. 4 for $V_B = 0.01V$. After a duration of about 140ps, the current density becomes essentially constant. The damped oscillation period is about 6ps. We remark that the time to equilibrate depends on the initial data preparation. The particle density and current density are displayed in Fig. 5. The particle density undergoes a very small change during evolution. The profile is slightly non-symmetric due to the applied voltage. In the mean time, the current density experiences an obvious initial layer, which keeps decaying afterwards. At $t = 90$ps, the variation is at about 1% of the average current density.

If we double the grid, namely, take $N = 1000$, the particle density remains almost unchanged during the evolution. See Fig. 7 at $t = 90$ps. However, the current density is more sensitive. Double grid leads to a much stronger initial layer, hence a longer time to equilibrate. See Fig. 6. Accordingly, the current density profile differs considerably with the $N = 500$ computing results at $t = 90$ps. Nevertheless, the average current density converges to the same steady state.

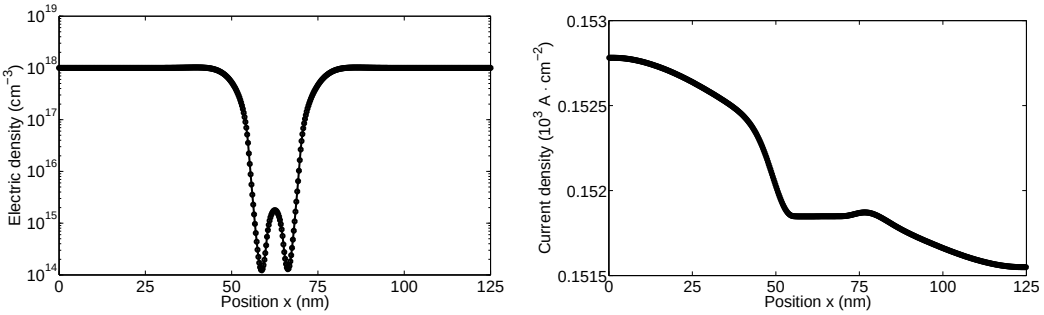

Figure 5: Particle density and current density by transient computations at $t=90$ps for $V_B=0.01$V.

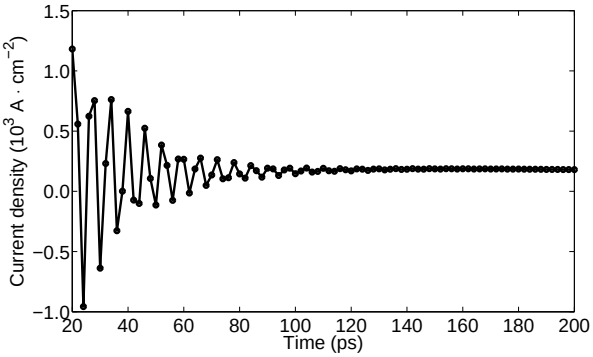

Figure 6: Current density (averaged in space) by transient computations at $V_B=0.01$V with double grid.

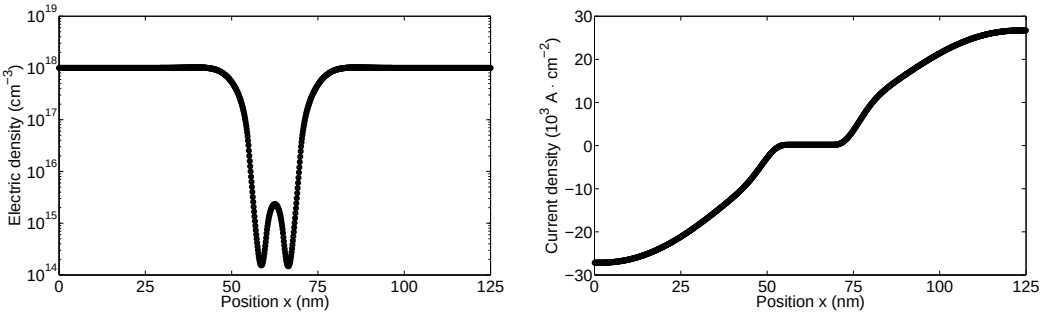

Figure 7: Particle density and current density by transient computations at $t=90$ps for $V_B=0.01$V with double grid.

In Fig. 8, we depict the transient current density at $V_B=0.15$V. After a duration of about 40ps, the current density becomes essentially constant. The damped oscillation period is about 5ps. In a later stage, the particle density and current density are displayed in Fig. 9. There is a charge accumulation between the barriers.

If we double the grid at this applied voltage, we find a quite different picture. In Fig. 10, although the initial layer decays in the first 20ps, there appears a seemingly non-decreasing temporal oscillation for current density. The period is about 65ps. The spatial variation remains big, as shown in Fig. 11 for $t=90$ps. Because we start the transient com-

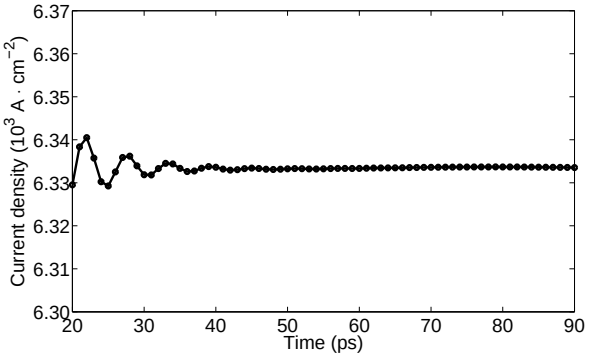

Figure 8: Current density (averaged in space) by transient computations at $V_B = 0.15$V.

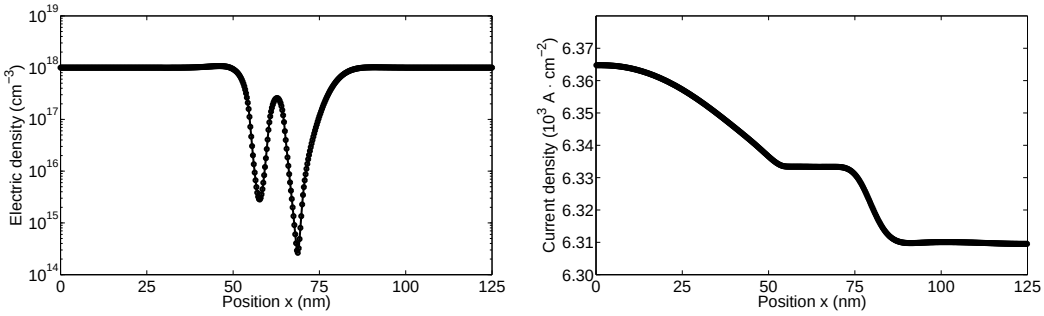

Figure 9: Particle density and current density by transient computations at $t = 90$ps for $V_B = 0.15$V.

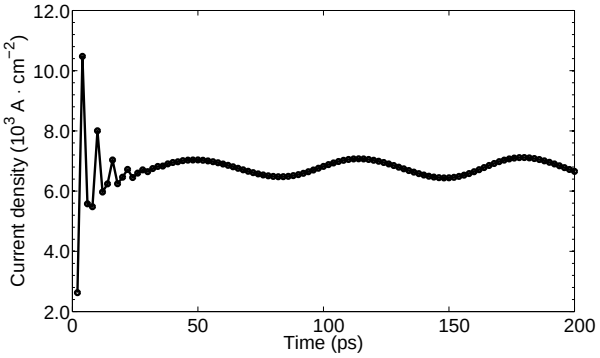

Figure 10: Current density (averaged in space) by transient computations at $V_B = 0.15$V with double grid.

putation from the steady state (with a perturbation), this obviously demonstrates that the steady state loses dynamical stability. If we view the semi-discrete transient system (3.1)-(3.3) as a dynamical system, the applied voltage V_B is the only control parameter. The steady state corresponds to a critical point. For small V_B, the critical point is stable, and the dynamical system converges to the critical point. At a larger applied voltage V_B (around 0.15V), the stationary solution becomes unstable. The temporally oscillating solution corresponds to a closed orbit.

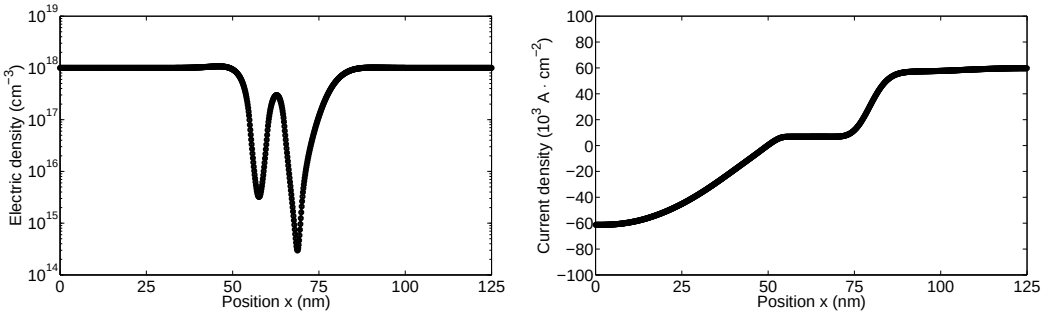

Figure 11: Particle density and current density by transient computations at $t=90$ps for $V_B=0.15$V with double grid.

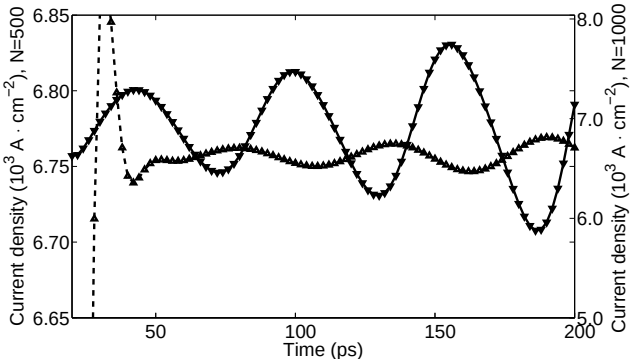

Figure 12: Current density (averaged in space) by transient computations at $V_B=0.19$V with 500 grid points (upward-triangle) and those with 1000 grid points (downward-triangle).

For larger applied voltages, the oscillations may grow indefinitely. At an applied voltage slightly higher than the NDR threshold, we see a persistent growth of the oscillation in Fig. 12 ($V_B=0.19V$). The oscillation period is again about 65ps. Nevertheless, the temporal average current density remains basically unchanged. Double grid results give rise to a higher amplitude, with a similar growing rate. We remark that when there is an oscillation in the current density, a temporal average is performed and displayed in the I-V curve in Fig. 3.

When we further increase the applied voltage, the oscillation becomes stronger with a larger growing rate. See Fig. 13. The period is always about 65ps. At even larger applied voltage, the numerical code breaks down. The stationary system still works for a bigger range, but also fails when applied voltage reaches about 0.22V. More careful study shows that there are accumulations of electrons around the boundary, and the Ohmic boundary conditions cause severe boundary layer. In this range, we are sceptical about the validity of the QHD model and the boundary condition for the one dimensional RTD. With a comparison to the vQHD model, we speculate that the energy equation with thermal diffusion is not enough to stabilize the QHD system. Rigorous mathematical analysis is desirable to substantiate understanding of the QHD model.

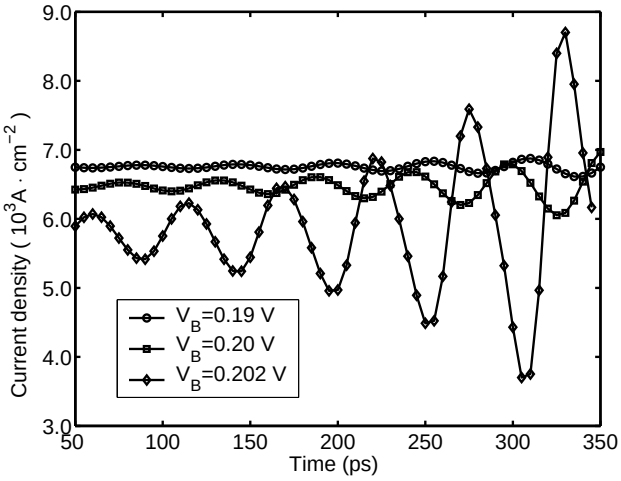

Figure 13: Current density (averaged in space) by transient computations at larger applied voltages.

5 Simulations for the QDD model

The QDD model (2.19)-(2.21) is easier to resolve numerically than the QHD model. We first rescale the system by

$$x \to Lx, t \to \frac{mL^2}{k_B T_0 \tau_0} t, n \to C_m n, C(x) \to C_m C(x),$$
$$V \to \frac{k_B T_0}{q} V, B(x) \to \frac{k_B T_0}{q} B(x), J \to \frac{k_B T_0 C_m \tau_0}{Lm} J.$$

Here $C_m = C(0) = 10^{18}\text{cm}^{-3}$. The undimensionalized QDD system reads

$$n_t + J_x = 0, \tag{5.1}$$
$$n_x - n(V+B(x))_x - \varepsilon^2 n \left(\frac{(\sqrt{n})_{xx}}{\sqrt{n}} \right)_x = -J, \tag{5.2}$$
$$\lambda^2 V_{xx} = n - C(x). \tag{5.3}$$

The scaled Planck constant ε and the Debye length λ are defined by

$$\varepsilon^2 = \frac{\hbar^2}{6mk_B T_0 C_m L}, \quad \lambda^2 = \frac{\epsilon_s k_B T_0}{q^2 C_m L^2}. \tag{5.4}$$

We introduce a quantum quasi Fermi level

$$F = -\varepsilon^2 \frac{(\sqrt{n})_{xx}}{\sqrt{n}} + \log n + (V + B(x)). \tag{5.5}$$

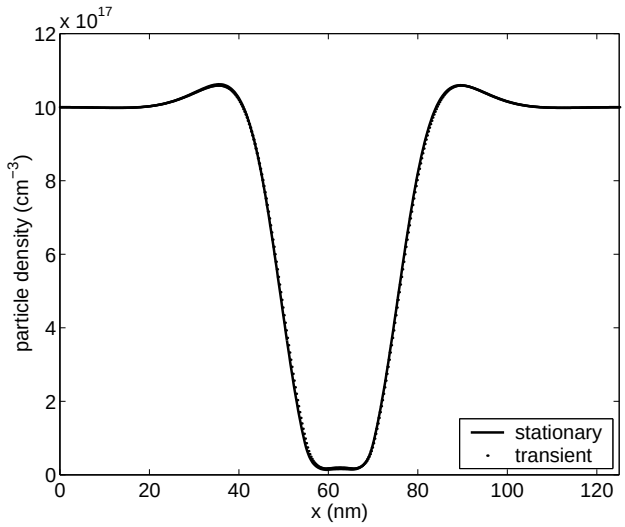

Figure 14: Particle density for QDD model at $V_B=0$V.

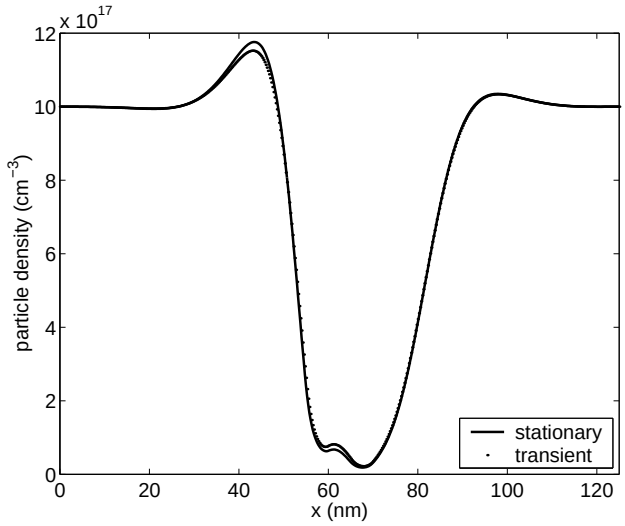

Figure 15: Particle density for QDD model at $V_B=0.3$V.

Here, the term $-\varepsilon^2(\sqrt{n})_{xx}/\sqrt{n}$ is the so-called quantum Bohm potential. Thus, we obtain the complete system of QDD model

$$n_t=(nF_x)_x, \tag{5.6}$$

$$-\varepsilon^2\frac{(\sqrt{n})_{xx}}{\sqrt{n}}+\log n+(V+B(x))=F, \tag{5.7}$$

$$\lambda^2V_{xx}=n-C(x). \tag{5.8}$$

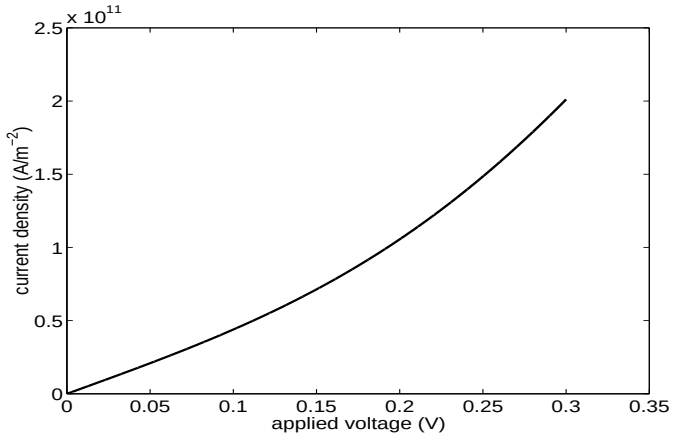

Figure 16: I-V curve by QDD model.

Furthermore, the current density J may be recovered from

$$J = -nF_x. \tag{5.9}$$

By a similar central difference and Newton-Raphson method, we simulate the transient and stationary problems. In contrast to the QHD model, the transient solution always converges, without oscillation. The difference between the two computations is quite small. In Figs. 14 and 15, we display the particle densities of both computations at two different applied voltages. The particle density distribution is symmetric at $V_B = 0$. Electrons tend to move along with the electric field for $V_B > 0$. Four humps appear. Two of them correspond to the doping boundary, and the other two correspond to the barriers.

From the I-V curve, we observe that the NDR phenomenon is not captured due to the strong diffusion in QDD. Actually, with a bipolar (two carriers) model, NDR was reported [23].

6 Discussions

In this paper, we have studied numerically the transient and stationary problems for fluid type models, including a QHD model and a QDD model. Different from a general perception that stationary simulations are enough for microelectronic devices, we discover that the quantum effects may influence charge transport in a more delicate manner for fluid type models. Steady states may lose stability and an incorrect I-V relation may be produced from the stationary computations. It is important to note that this instability could occur at an applied voltage that falls into the operation range of the quantum device. We believe that transient computations are necessary for quantum charge transport simulations with fluid type models in general.

Acknowledgments

We would like to thank the anonymous referee for stimulating discussions. This research is partially supported by NSFC under grant No. 90407021, National Basic Research Program of China under contract number 2007CB814800, and the China Ministry of Education under contract number NCET-06-0011.

References

[1] P. Antonelli and P. Marcati. On the finite energy weak solutions to a system in quantum fluid dynamics. Preprint (`http://arxiv.org/PS_cache/arxiv/pdf/0802/0802.0846v1.pdf`), 2008.
[2] A. Arnold, J.L. López, P. Markowich, and J. Soler. An analysis of quantum Fokker-Planck models: A Wigner function approach. Rev. Mat. Iberoam., 20(3) (2004), 771-814.
[3] P. Caussignac, J. Descloux, and A. Yamnahakki. Simulation of some quantum models for semiconductors. Math. Models Meth. Appl. Sci., 12 (2002), 1049-1074.
[4] L.L. Chang, L. Esaki and R. Tsu, Resonant tunneling in semiconductor double barriers, Appl. Phys. Lett., 24 (1974), 593.
[5] Z. Chen. A finite element method for the quantum hydrodynamic model for semiconductor devices. Computers Math. Appl., 31 (1996), 17-26.
[6] Z. Chen, B. Cockburn, C.L. Gardner, and J.W. Jerome. Quantum hydrodynamic simulation of hysteresis in the resonant tunneling diode, J. Comp. Phys., 117 (1995), 274-280.
[7] Z. Chen, B. Cockburn, J.W. Jerome, and C.-W. Shu. Mixed-RKDG finite element methods for the 2-D hydrodynamic model for semiconductor device simulations, VLSI Design, 3 (1995), 145-158.
[8] C. de Falco, E. Gatti, A.L. Lacaita, and R. Sacco, Quantum-corrected drift-diffusion models for transport in semiconductor devices, J. Comput. Phys., 204 (2005), 533-561.
[9] P. Degond and C. Ringhofer. Quantum moment hydrodynamics and the entropy principle, J. Stat. Phys., 112 (2003), 587-628.
[10] W. R. Frensley, Boundary conditions for open quantum systems driven far from equilibrium, Reviews of Modern Physics, 62 (1990), 745-791.
[11] C. Gardner. The quantum hydrodynamic model for semiconductor devices, SIAM J. Appl. Math., 54 (1994), 409-427.
[12] M.P. Gualdani and A. Jüngel. Analysis of the viscous quantum hydrodynamic equations for semiconductors, Europ. J. Appl. Math., 15 (2004), 577-595.
[13] H.K. Gummel, A self-consistent iterative scheme for one-dimensional steady state transistor calculations, IEEE Trans. Elec. Devices, 11 (1964), 455-464.
[14] X. Hu, and S.Q. Tang, Transient and stationary simulations for a quantum hydrodynamic model, Chin. Phys. Lett., 24 (2007), 1437-1440.
[15] International Technology Roadmap for Semiconductors, ITRS Report Modelling and Simulation, `http://public.itrs.net`, 2005.
[16] A. Jüngel, Quasi-hydrodynamic Semiconductor Equations, Birkhäuser, Basel, 2001.
[17] A. Jüngel, D. Matthes, and J.P. Milišić, Derivation of new quantum hydrodynamic equations using entropy minimization, SIAM J. Appl. Math., 67 (2006), 46-68.
[18] A. Jüngel, and S. Tang, Numerical approximation of the viscous quantum hydrodynamic model for semiconductors, Appl. Numer. Math., 56 (2006), 899-915.

[19] H.L. Li, G.J. Zhang, and K.J. Zhang, Algebraic time-decay for the bipolar quantum hydrodynamic model, Math. Models Method Appl. Sci., 18(6) (2008), 859-881.
[20] E. Madelung. Quantentheorie in hydrodynamischer Form, Z. Physik, 40 (1927), 322-326.
[21] P. Markowich, C. Ringhofer, and C. Schmeiser, Semiconductor Equations, Springer, Vienna, 1990.
[22] Y. Peng, Y.G. Wang, and W.A. Yong, Quasi-neutral limit of the non-isentropic Euler-Poisson system, Proc. Roy. Soc. Edinburgh, 136A (2006), 1013-1026.
[23] R. Pinnau, and A. Unterreiter, The stationary current-voltage characteriztics of the quantum drift-diffusion model, SIAM J. Numer. Anal., 37 (1999), 211-245.